

FUNCTIONAL DIVERSITY OF MOTONEURON DENDRITES: BY ACCIDENT OR DESIGN?

P.K. ROSE*, S. CUSHING, G. GRANDE AND T. BUI

*CIHR Group in Sensory-Motor Integration, Department of Physiology, Center for Neuroscience,
Queen's University, Kingston, ON, Canada K7L 3N6*

INTRODUCTION

Spinal motoneurons have a distinct dendritic tree (3, 12, 15, 16, 17, 20, 31, 34, 35, 41, 45, 47, 51, 52). Most spinal motoneurons have 8 to 14 primary dendrites that give rise to arborizations consisting of up to 10 orders of branching. Together, these arborizations form a multi-trunk tree that spreads throughout much of the ventral horn and spans distances of 2 to 4 mm. Ramón y Cajal (40) was the first to recognize that the distribution of motoneuron dendrites, despite the complexity of the dendritic tree, is not random. Instead, dendritic trees of motoneurons form highly stereotyped distribution patterns that depend on the location of the motoneuron nucleus. More recent studies, based on intracellular or retrograde staining techniques, have confirmed and extended the observations of Ramón y Cajal (6, 11, 18, 24, 29, 36, 41, 42, 53, 55). Further evidence of a precise pattern in the distribution of motoneuron dendrites can be found in the organization of the subtrees formed by the branches arising from primary dendrites. These subtrees occupy discrete zones (18, 42) (see (4) for a similar analysis of cranial motoneurons). Within a single motor nucleus, the frequency of individual classes of subtrees, as defined by their projection zones, is remarkably consistent from motoneuron to motoneuron (42).

The rules governing the quantitative geometry of spinal motoneurons appear to be as stringent as the rules that determine the distribution of their dendrites. Many studies have demonstrated that the combined length or surface area of subtrees originating from primary or second-order dendrites are correlated with the diameters of primary or second-order dendrites (10, 12, 17, 30, 45, 47, 51, 52). The parameters of the regression equations that describe these relationships depend on the trajectory followed by the dendrites (45). For example, the slope of the relationship between the combined surface areas of subtrees that project rostrally or caudally from trapezius motoneurons is two to three times larger than the slope of the same relationship for subtrees that project in other directions. Thus, quantitative geometrical properties of spinal motoneuron dendrites are related to their distribution pattern.

The present studies are based on the premise that there is a functional counterpart to the highly ordered structure of motoneuron dendritic trees. These studies were inspired by a seminal paper published by Tyc-Dumont and her colleagues in 1987

* Corresponding Author: Dr. P.K. Rose, Department of Physiology, Queen's University, Kingston, ON, Canada, K7L 3N6 - Tel: +613 533-2804 - Fax: +613 533-6840 - E-mail: ken@biomed.queensu.ca

(4). This report extended theoretical studies of the transmission of synaptic signals along dendrites (32, 38) to 'real' motoneurons, that is motoneurons whose structure was defined, not by arbitrary cylinders with an assumed length and diameter, but by precise measurements of the dendritic geometry of intracellular stained and electrophysiologically motoneurons. The results of this study and subsequent investigations (7, 19) established that the functional properties of motoneuron dendrites, as defined by their ability to deliver synaptic current and voltage changes to the soma and local interactions between neighbouring synapses, are as variable as the structural properties of motoneurons. Our goal is to demonstrate that there is a pattern in this diversity, based in part on the trajectory followed by the dendrites, which leads to a functional organization of motoneuron dendrites that is not random, but instead is designed to divide the dendritic tree into functional subunits.

METHODS

Experimental procedures

The motoneurons used in the present study were selected from a collection of motoneurons stained in previous experiments (44, 46). The experimental protocols were approved by the Queen's University Animal Care Committee and were consistent with guidelines established by the Canadian Council of Animal Care. Motoneurons were identified antidromically by stimulating nerves that supply the dorsal neck muscles of adult cats. The methods for intracellular staining and tissue processing have been described in detail elsewhere (43).

Measurement of dendritic geometry and classification of dendritic trajectories

Dendritic trees were reconstructed using a Wild-Leitz microscope equipped with a X63 oil immersion objective (N.A.1.40) and a Eutectic neuron tracing system (13, 43). Each motoneuron fulfilled the following criteria: distal dendrites could be traced to abrupt terminations, as opposed to a gradual, proximal to distal, loss of staining; dendritic beading was absent; there was no evidence of damage to the soma; differential shrinkage where the tissue shrinks more than the stained process, leading to curling of dendrites that travel in the Z-axis (27), was absent.

Starting at a dendritic terminal, each dendrite was followed back to the soma. The trajectory of the dendritic branches between the soma and the dendritic terminal was classified according to its predominate three-dimensional orientation. In general, classification was straight-forward, since most trajectories had long paths orientated close to one or two of the three primary directions: rostral/caudal, dorsal/ventral and medial/lateral. For 'border-line' cases, we followed two rules: i) directions were distinguished by zones, 45 degrees wide, that spanned ± 22.5 degrees from a primary direction or any combination of two primary directions, and ii) a direction was included only if at least 30% of the trajectory followed that orientation. Trajectories with similar directions in the transverse plane (e.g. dorsal-lateral) and a component in the rostral or caudal direction were grouped together, since the trajectories of these dendrites, when viewed in the transverse plane, occupied the same region of the spinal cord.

Construction of compartmental models

Compartmental models were constructed as delineated previously (7). The number of compartments ranged from 4,000 to 5,000. Unless otherwise stated, specific internal resistivity was set at $70 \Omega\text{cm}$, the value of specific membrane capacitance was $1 \mu\text{Fcm}^{-1}$ and specific membrane resistivity (R_m) was fixed at $15,000 \Omega\text{cm}^2$.

Most models were passive, i.e. no voltage-dependent channels. However, in some simulations,

we incorporated L-type calcium channels as described in⁷. Briefly, L-type Ca^{2+} channels were modeled as a maximal conductance per surface area ($g_{\text{L,Ca}}$).

$$g_{\text{L,Ca}} = g_{\text{peak}} m \quad (1)$$

where m is a voltage- and time dependent activation variable. The activation variable was modeled by the differential equation:

$$\frac{dm}{dt} = \frac{m_{\infty} - m}{t_m} \quad (2)$$

where the time constant of activation, t_m , was set at 20 ms. The steady-state activation level, m_{∞} , is described by the equation:

$$m_{\infty} = \frac{1}{1 + e^{(V_m - V_{1/2})/k}} \quad (3)$$

where the half-activation voltage ($V_{1/2}$) was set at -33 mV and the activation sensitivity, k , was assigned a value of -6 mV. E_{rev} for the calcium current was set at 60 mV.

The conductance change caused by each synapse was modelled by means of the following equation (cf. (1)):

$$g(t) = g_{\text{peak}} (t/t_{\text{peak}}) \exp[1 - (t/t_{\text{peak}})] \quad (4)$$

For excitatory synapses, t_{peak} was set at 0.2 msec and g_{peak} was assigned a value of 5.0 nS (21). For inhibitory synapses, t_{peak} and g_{peak} were increased to 0.65 msec and 9.0 nS, respectively. These values correspond to the time course and magnitude of the conductance caused by activation of single axons of Ia inhibitory interneurons (50). To mimic tonic, asynchronous activation of many synapses, these time-dependant synaptic conductances were replaced by a constant, equivalent time-averaged conductance change, \bar{g} , as described by (1). \bar{g} is the integral of $g(t)$ where:

$$\bar{g} = g_{\text{peak}} t_{\text{peak}} \exp(1) n f P_{\text{release}} \quad (5)$$

n is the number of synapses, f is the activation frequency and P_{release} is the probability of neurotransmitter release (cf. (54)).

Simulations were performed using Saber, a mixed-signal simulator software package (Synopsys Inc., Mountain View, CA) (14).

RESULTS

Diversity of the efficacy of transmission of synaptic signals along motoneuron dendrites

It is well known that dendrites act as leaky electrical cables (32, 38). As a consequence, current generated by dendritic synapses is lost en route to the soma. This loss, coupled with larger input resistances at dendritic sites, compared to the soma, leads to large attenuations in the voltage change caused by dendritic synapses as the voltage change travels towards the soma (39). To determine the attenuation of current and voltage signals along the dendrites of motoneurons, we measured the change

in steady-state current and voltage in all compartments in response to current injection at the soma or dendritic terminals. Voltage attenuation en route to the soma from compartment X (V_{att_X}) was defined by:

$$V_{att_X} = V_X/V_{soma} \quad (1)$$

where V_X is the change in voltage in compartment X and V_{soma} is the change in the somatic voltage in response to current injected in a dendritic terminal, distal to X. As described by⁴, current attenuation en route to the soma (I_{att_X}) is:

$$I_{att_X} = V_{att_X} (R_N/R_X) \quad (2)$$

where R_N is the input resistance of the neuron, measured at the soma and R_X is the input resistance at compartment X. This means of calculating current attenuation is equivalent to determining the ratio of injected current to the current reaching a voltage clamped soma.

As shown in Table 1, the attenuation of voltage and current signals en route from the dendritic terminal to the soma varied widely. As an index of this variability, we used the ratio of the 75th to 25th percentile. For V_{att} (terminal to soma), the 75th percentile exceeded the 25th percentile by almost 100 fold. The range of values of I_{att} (terminal to soma) was smaller, but the 75th percentile still exceeded the 25th percentile by 2 fold. The input resistance as seen from the dendritic terminals was also highly variable.

Despite the widespread use of I_{att} (terminal to soma) and V_{att} (terminal to soma) as indices of the overall morphoelectronic properties of neurons, they are biased to the most extreme values. I_{att_X} and V_{att_X} of compartments en route to the soma will be smaller. Since the density of synapses on neck motoneuron dendrites is relatively uniform (46), more proximal dendritic segments, due to their larger diameter, will receive more synapses. Thus, the attenuation of voltage and current signals generated by an 'average' synapse, located somewhere between the soma and a dendritic ter-

Table 1. - *Variability in functional properties of neck motoneuron dendrites**

Parameter	25 th percentile	median	75 th percentile
V_{att} (terminal to soma)	3.67	139.6	370.5
I_{att} (terminal to soma)	1.29	1.78	2.82
R_d (at terminal, MW)	141.4	402.1	770.8
V_{att} (AW)	5.5	14.3	29.2
I_{att} (AW)	1.10	1.26	1.62
R_d (AW)	21.4	46.5	86.6
EPSP _{att} (AW)	37.6	103.0	240.2
EPSP rise time (AW, msec)	0.64	1.12	1.87
EPSP half-width (AW, msec)	3.98	5.62	10.41

Based on measurements of 548 trajectories (the path followed from the soma to a dendritic terminal) that formed the dendritic trees of four neck motoneurons, see (7) for further details.

minal, will be biased to I_{att_x} and V_{att_x} of proximal compartments. To address this concern, we calculated 'area-weighted' versions of attenuation factors that took into account the area and I_{att_x} or V_{att_x} of all compartments en route to the soma from each dendritic. These area weighted attenuation factors, $I_{att}(AW)$, and $V_{att}(AW)$, were the sum of I_{att_x} or V_{att_x} for all compartments, after normalization by area, found along the path of each dendritic trajectory from the soma to its termination:

$$I_{att}(AW) = \Sigma I_{att_x} (area_x / Sarea_x) \quad (3)$$

and

$$V_{att}(AW) = \Sigma V_{att_x} (area_x / Sarea_x) \quad (4)$$

Assuming that synapse density is uniform, $I_{att}(AW)$ and $V_{att}(AW)$ are, respectively, equivalent to the average steady-state attenuation en route to the soma of the current and voltage signals generated by all synapses on a given trajectory (see (7) for further discussion of the merits and limitations of area weighting). Calculations of an area-weighted version of input resistance for each dendritic terminal to soma trajectory, $R_D(AW)$, were performed in a similar manner. The area-weighted versions of V_{att} , I_{att} and R_D varied less than their terminal counterparts, but there was still large differences between the 25th and 75th percentiles (Table 1). We also calculated area-weighted versions of the voltage attenuation of EPSPs en route to the soma and the rise-times and half-widths of the EPSPs as recorded at the soma. These parameters also displayed a high degree of variability, especially voltage attenuation (Table 1).

The wide variability in the transmission of steady-state and transient synaptic signals by dendrites of neck motoneurons is consistent with the results reported by Tyc-Dumont and her colleagues (4, 34). Thus, both spinal and cranial motoneurons display a functional diversity, as defined by their efficacy of transmission of synaptic signals that is as rich as their structural diversity. This result is a critical first step in testing the hypothesis that the functional properties of motoneuron dendrites, like the structural properties, are governed by specific rules that impose an order to the variability. Without this variability, there would be little point in pursuing the premise further.

Relationship between the efficacy of transmission of synaptic signals along motoneuron dendrites and their trajectory

Dendritic geometry is related to the trajectory followed by neck motoneuron dendrites (45). In the absence of voltage-dependent channels, current and voltage attenuation, as well as local input resistance, also depend on dendritic geometry (38). Thus, the current and voltage reaching the soma should depend on the trajectory of the dendrites. Our second goal was to test this hypothesis. To achieve this objective, we took advantage of the highly organized distribution of dendrites arising from biventer cervicis and complexus (BCCM) motoneurons (41, 42). The dendrites of BCCM motoneurons are arranged in three distinct groups. One group projects rostrally or caudally to form a dense collection of dendrites within the motor nucleus.

The other two groups, respectively, travel dorsolaterally and dorsomedially. As shown in Figure 1, trajectories with a rostral or caudal component were divided into 5 classes, based on the presence or absence of additional dorsal and/or medial or lateral components. Thus, dendrites travelling only in a rostral or caudal direction (R/C) were distinguished from those with an additional dorsal (R/C-D) or lateral (R/C-L) component, or components travelling dorsal-laterally (R/C-D-L) or dorsal-medially (R/C-D-M). The projections of the remaining 5 classes of trajectories were confined to the transverse plane and included trajectories travelling medially (M) or dorsally (D) or laterally (L) or dorsal-laterally (D-L) or dorsal-medially (D-M). Most trajectories belonged to the 5 classes with a rostral or caudal component (73% of classified trajectories) and, of these, almost one-half travelled only rostrally or caudally (R/C). Most trajectories that were confined to the transverse plane projected dorsal-medially (D-M) or dorsal-laterally (D-L) or laterally (L).

Values for $I_{att}(AW)$ and $V_{att}(AW)$ (after standardization to remove between-cell variability) are organized by trajectory and displayed in the form of box plots in Figure 2. An analysis of variance demonstrated that the ability of motoneuron dendrites to deliver current to the soma depends on their trajectory ($P < 10^{-15}$ for $I_{att}(AW)$, $P=0.0006$ for $V_{att}(AW)$, $P=0.06$ for $R_D(AW)$, data not shown). However, this analysis does not indicate if current attenuation is systematically related to particular features of the trajectory (eg. a rostral or caudal orientation). To address this question, we exploited hierarchical cluster methods (see (43) for further details). The box plots in Figure 2A are rearranged and colour coded according to the results of the cluster analysis. This analysis identified three principal groups of trajectories based on $I_{att}(AW)$. One group consisted of dendrites with a rostral or caudal component in their trajectory (R/C, R/C-D, R/C-D-M). These trajectories were grouped together as a consequence of their high current attenuations. Dendrites with R/C-D-L, D-M and D trajectories had current attenuations that were mid-way between the high current attenuation cluster and a cluster consisting of R/C-L, D-L, L and M trajectories. The latter cluster had the lowest current attenuations. Cluster analysis of the $V_{att}(AW)$ data divided the trajectories into two groups, one with high voltage attenuations and the other with low voltage attenuations (Figure 2B). The trajectories belonging to the high voltage attenuation cluster had a dorsal or rostral/caudal component in their trajectory. The low voltage attenuation cluster was dominated by dendrites with a lateral component in their trajectories (L, D-L, R/C-L). As a consequence, three of the four trajectories belonging to the low voltage attenuation cluster formed a contiguous zone, lateral to the somata of BCCM motoneurons, similar to trajectories belonging to the low current attenuation cluster.

Based on the results of the cluster analysis, the trajectories belonging to each $I_{att}(AW)$ cluster were combined and their distribution patterns were compared. As shown in Figure 3, dendrites belonging to each cluster were arranged in distinct zones within the ventral horn. Trajectories belonging to the high $I_{att}(AW)$ cluster formed a network of dendrites that stretched rostrally and caudally from the soma. Many of these dendrites were confined to the base of the ventral horn, but some also

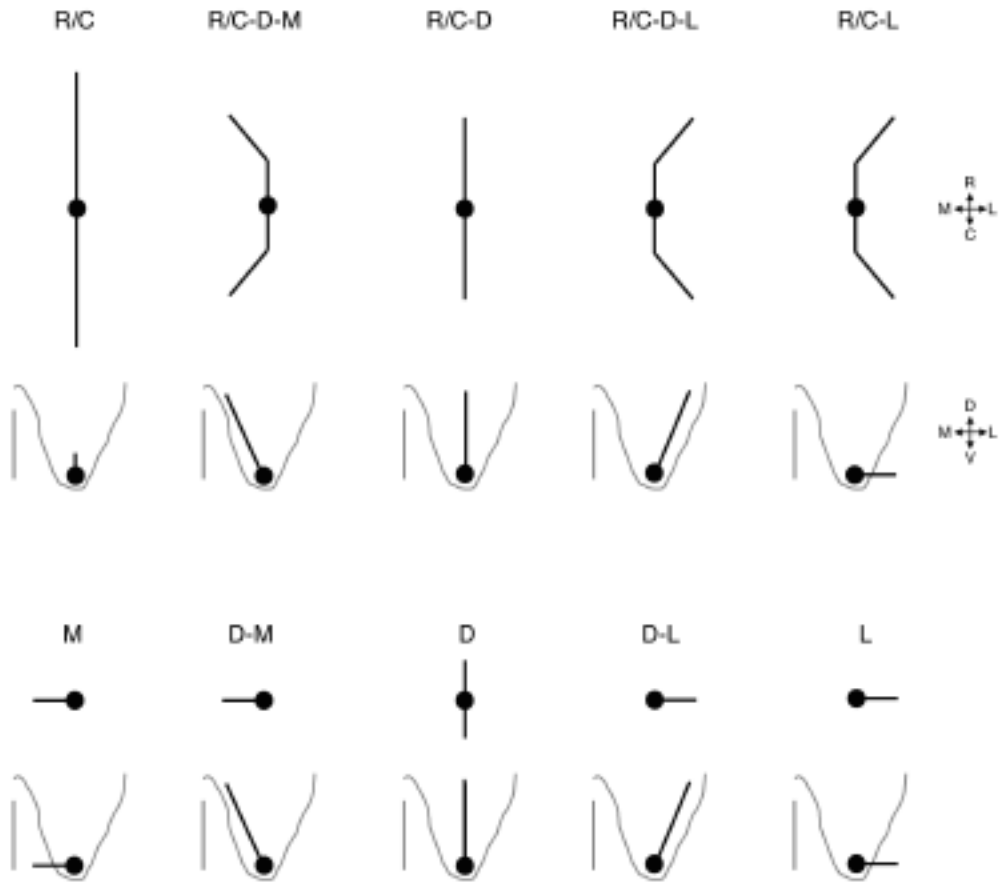


Fig. 1. - Schematic representation of the distribution of dendrites belonging to each trajectory.

The upper panel shows the five classes of trajectories with a rostral or caudal component. The lower panel shows the remaining five classes of trajectories. All trajectories are shown in the horizontal (upper row) and transverse (lower row) planes. The direction 'vanies' to the right of the R/C-L trajectory apply to all trajectories. R-rostral, C-caudal, M-medial, L-lateral, D-dorsal, V-ventral

projected dorsally, especially along the medial side of lamina VIII. In contrast, most trajectories that were part of the intermediate and low Iatt(AW) clusters occupied a rostral-caudal zone closer to the soma. Despite this similarity, there were distinct differences in the three-dimensional distribution pattern of trajectories belonging to these clusters. These differences were most apparent when viewed in the transverse plane.

Relationship between the interaction of neighbouring synapses and the trajectory of motoneuron dendrites

The current delivered by an ionotropic synapse is determined by the product of two factors: the conductance change caused by opening of ligand-dependent chan-

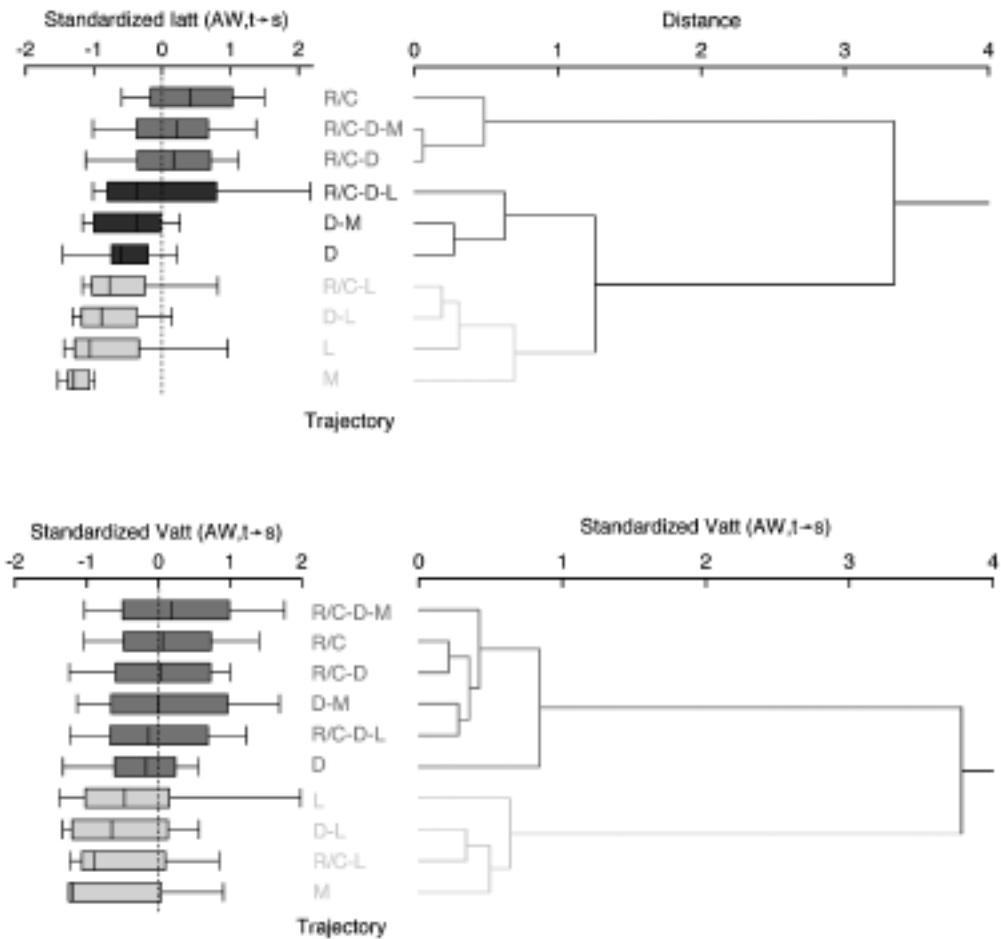


Fig. 2. - (A) Cluster analysis of trajectories based on $I_{att}(AW, \text{terminal to soma})$. Box plots of standardized values of $I_{att}(AW, \text{terminal to soma})$, shown on the left, color coded according to the results of a hierarchical cluster analysis shown on the right.

Hierarchical cluster analysis provides a graphical index of the similarity or differences between trajectories belonging to the same or different clusters according to the distribution of the standardized values of $I_{att}(AW, \text{terminal to soma})$. The X-axis (distance) is a measure of the similarity (short distance) or difference (long distance). (B) Cluster analysis of trajectories based on $V_{att}(AW, \text{terminal to soma})$. Same format as A.

nels and the driving potential (the difference between the equilibrium potential and the instantaneous membrane potential). The dependence on driving potential imposes an intrinsic non-linearity on the summation of synaptic currents and the resulting postsynaptic potentials generated by two or more simultaneously active synapses. The goal of this stage of the study was to compare the impact of this non-linearity on the input-output properties of dendrites classified by their trajectory (i.e. rostral/caudal versus dorsomedial) where the input is defined by the number and proportion of

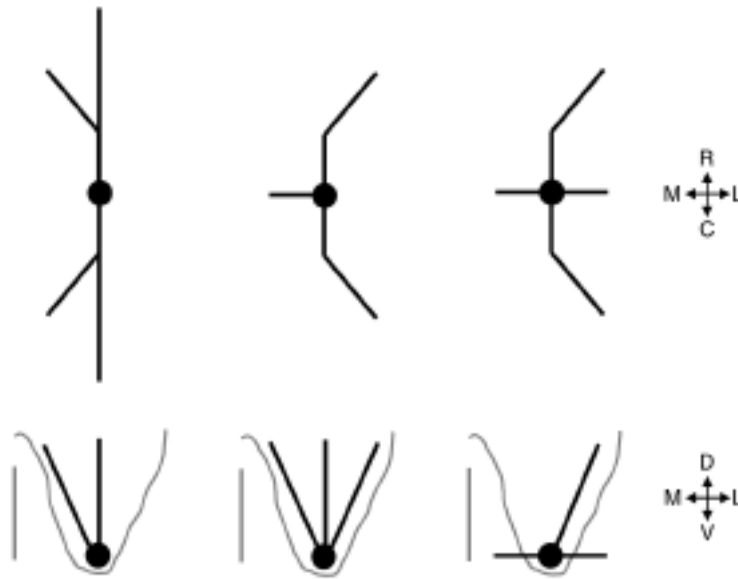


Fig. 3. - Schematic representation of the distribution of trajectories belonging to the high $I_{att}(AW)$, terminal to soma) cluster (left), intermediate $I_{att}(AW)$, terminal to soma) cluster (middle), and low $I_{att}(AW)$, terminal to soma) cluster (right), shown in the horizontal (top) and transverse (bottom) planes. R-rostral, C-caudal, M-medial, L-lateral, D-dorsal, V-ventral.

active excitatory and inhibitory synapses and the output is defined by the current reaching the soma. Current was measured using the same protocol developed by (25) and widely used by Binder and colleagues (2). This protocol has two distinct advantages. First, the current reaching the soma is the primary factor governing the steady-state frequency of action potentials generated by a tonic barrage of presynaptic activity (22, 23, 48) (for a review see (2)). Secondly, in a simulation, synapses can be represented by constant current injection devices (i.e. constant driving potential) or ‘physiological’ synapses where the driving potential depends on the local membrane potential. Thus, we could directly compare the current lost due to non-linear summation versus that lost due to leakage en route to the soma.

All simulations were based on the same compartmental models constructed in the previous analysis. Dendrites belonging to a single trajectory class were identified based on the same criteria as before and synapses were uniformly distributed, i.e. same number of synapses per unit area, on these dendrites. Synaptic densities of excitatory synapses were limited to a maximum of one synapse/ $28.6\mu\text{m}^2$ based on previous electron microscopic observations (46). The positions of the synapses were assigned using the following protocol. Beginning at the cell body, the cumulative area of successive compartments was determined. If addition of the next distal compartment resulted in a cumulative area exceeding a pre-defined value (e.g. for a density of 2% of the maximum number of excitatory synapses, there is one

synapse/ $1430\mu\text{m}^2$), a synapse was randomly placed in that compartment or in one of the proximal compartments that contributed to the pre-defined area value. If the cumulative area exceeded the pre-specified area value, \bar{g} was adjusted to take into account the “excess area” contributed by the distal compartment. At low synaptic densities, the area of the last sequence of compartments that included the termination of a dendrite was invariably less than the pre-defined area interval. A ‘partial’ synapse was randomly assigned to one of these compartments, where \bar{g} was determined by the ratio of the area of the compartments to the pre-defined area interval. The random assignment of synapses to the compartments contributing to each pre-specified area was designed to avoid a systematic bias in synapse location that would have occurred if the synapses were placed on either the first or last compartment within each pre-specified area zone. An alternative scheme whereby each compartment was assigned a fraction of a synapse, based on the area of the compartment would have achieved the same goal, but was rejected because it conflicted with our goal of building a model that was as anatomically realistic as possible.

Figure 4 compares the current reaching the soma following activation of synapses on R/C, R/C-D-L and D-L dendrites of one motoneuron. The magnitude of current reaching the soma is shown for three different conditions. In the first condition, all synapses were arbitrarily placed on the soma and assigned a constant driving potential (i.e. equivalent to constant current injection devices). As expected from the parameters assigned to each synapse (see Methods), each synapse delivered 8.7 pA to the soma. In the second condition, the synapses were distributed uniformly such that the number of synapses per 100 mm^2 was the same throughout the somato-dendritic surface of the cell. Under these conditions, the same synapses delivered less current to the soma due to the current lost en route to the soma due to the cable properties of the dendrites. In the final condition, the synapses were also distributed uniformly, but the constraint of a constant driving potential was removed. Instead, the driving potential was determined by the local membrane potential at the site of each synapse. Under these conditions, the relationship between the number of active synapses and the current reaching the soma was non-linear. This decrease was a direct result of current lost (indicated by the gray zone in Figure 4A, 4B and 4C) due to decreases in the driving potential. As indicated by the progressively large size of this zone in Figures 4A, 4B and 4C, the current lost due to decreases in driving potential depended on the trajectory of the dendrites.

The second derivative of the current reaching the soma based on physiological synapses is equal to the current lost due to non-linear summation with each successive synapse (see (19) for more details). Figure 4D compares the current lost due to non-linear summation following successive activation of 1% of the total number of synapses on R/C, R/C-D-L and D-L dendrites. This loss was highest on R/C dendrites, intermediate on R/C-D-L and dendrites and least on D-L dendrites. At the lowest levels of synaptic activity, the loss of current due to non-linear summation was 2.6 fold higher on RC dendrites compared to R/C-D-L dendrites and over 9 fold greater on R/C dendrites compared to D-L dendrites. The differences in the current lost due to non-linear summation between the trajectories decreased as the intensity

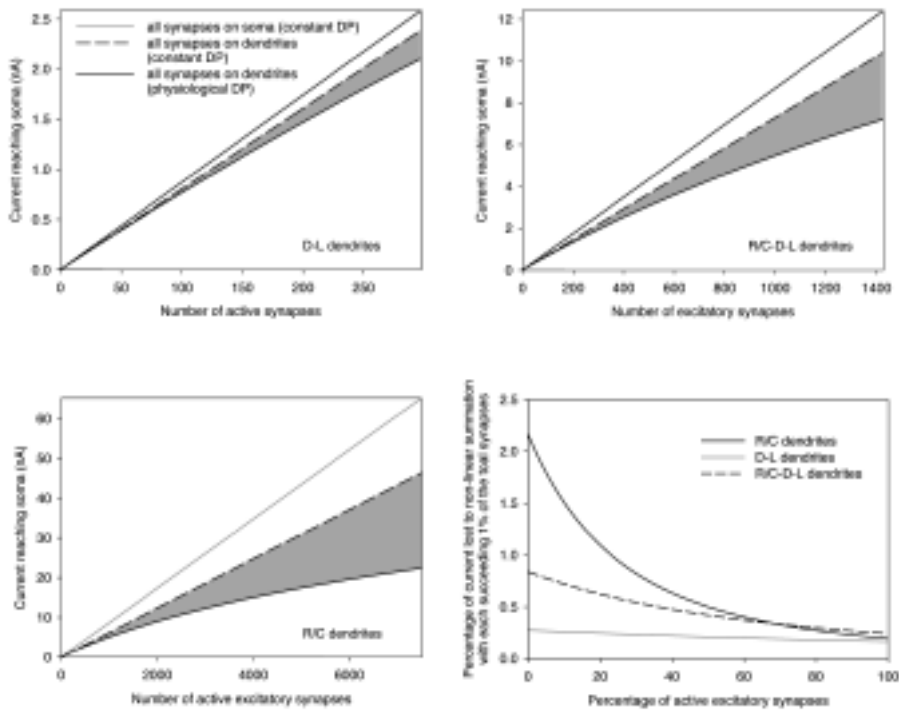


Fig. 4. - *Input-output properties of dendrites belonging to different trajectories.*

A-C: Relationships between the number of active excitatory synapses on D-L, R/C-D-L and R/C dendrites and the current reaching the soma. The legend in A also applies to B and C (DP – driving potential). All synapses were activated at 100 Hz with $P_{\text{release}} = 0.5$. The grey zone illustrates the loss of current due to decreases in driving potential. D: Loss of current due to non-linear summation following activation of successive groups of synapses where each group consisted of 1% of the total number of synapses. This loss was expressed as the percentage of the current reaching the soma in the absence of non-linear summation. Note that the loss depended on the trajectory of the dendrites.

of synaptic activity rose, such that at very high levels of synaptic activity, all trajectories were approximately equivalent in terms of the current lost due to non-linear summation.

DISCUSSION

This study was founded on the principle that the functional properties of motoneurons dendrites, as defined by their ability to deliver current and voltage signals from synapses on the dendritic tree to the soma are not random, but instead are closely related to the trajectory followed by the dendrites. Our analysis of numerous parameters that describe the transmission of signals along motoneuron dendrites (e.g. attenuation of steady state current and voltage signals) indicated that these parameters display a wide degree of variability. These results were based on an examination

of the dendritic tree *as a whole* and therefore closely paralleled previous studies on cranial motoneurons by Tyc-Dumont and colleagues (4, 5, 33, 34) that reached the same conclusions. This variability was a necessary and critical criterion for our central hypothesis. Without this variability there would be little justification for seeking a relationship between these properties and structural properties of motoneuron dendrites, specifically the trajectory they follow from their soma to their termination. This analysis revealed that the efficacy of transmission of steady-state synaptic signals is indeed strongly related to dendritic trajectory. This relationship extends beyond the transmission of signals generated by a single synapse to include non-linear interactions between neighbouring co-active synapses. These interactions amplify the differences in transmission efficacy between dendritic trajectories as seen following activation of single synapses.

All of the simulations conducted in the present study were based on the assumption that membrane properties of motoneurons are passive, i.e. not voltage-dependent. This strategy was intentional, despite the fact that this assumption is incorrect (26, 37). Our primary goal was to determine if trajectory-related differences in dendritic geometry, could, *by themselves*, lead to differences in the transmission of signals to the soma. The fact that this hypothesis proved to be correct provides a strong justification for this approach (see also (28) for a discussion of the importance of dendritic geometry as a means of reducing or eliminating distance dependent differences in the size of synaptic potentials recorded at the soma). It is important to emphasize however, that our analysis of the transmission of signals by the dendrites of neck motoneurons is only the first step along the path towards a full understanding of the integrative properties of these cells. Recent studies have incorporated local 'hot-spots' of voltage-dependent calcium channels into compartmental models of the same cells used in the on the present study (8). Despite an identical distribution of the hot-spots, the hot-spots were recruited a widely different levels of excitatory synaptic activity. Thus, differences in the transmission of signals to the soma are also a property of active models. Whether these differences match those reported here is not known, but by beginning the analysis of signal transmission based on passive properties, we have established a foundation upon which the complex non-linear actions of voltage-dependent channels can be properly interpreted.

In the present studies, specific membrane resistivity was not varied (although the effective resistivity was changed in the studies of non-linear summation of synaptic current delivered to the soma). Previous studies have demonstrated that decreasing R_m can dramatically alter the electrical compactness of motoneurons (34). At very high levels of background synaptic activity ($R_m = 1000 \Omega\text{cm}^2$), synaptic inputs located more than 500 μm from the soma are electrically 'disconnected' from the soma. At low levels of background synaptic activity ($R_m = 100,000 \Omega\text{cm}^2$), all synaptic inputs, regardless of their distance from the soma, have charge (equivalent to current in this context) attenuation factors of less than 2. These findings led to the proposal that the dendritic trees of motoneurons are organized into two functional regions, one proximal to the soma, the other distal.

The boundary (i.e. distance from the soma) between these regions is very sensitive to R_m . In a related study (33), the efficacy of signal transmission was described on a branch by branch basis. This analysis revealed a similar proximal to distal organization of functional subunits. Moreover, as R_m was decreased from 10,000 Ωcm^2 to 3000 Ωcm^2 to 1000 Ωcm^2 , almost 3 in 10 dendritic branches switched from one functional subunit to another. Thus, based on previous studies, functional subunits within the dendritic trees of motoneurons are organized into proximal versus distal domains and the spatial organization of these domains depends on the level of background synaptic activity.

In contrast, the organization of functional subunits described in the present study was based on dendritic orientation. It is important to recognize that functional subunits described in this study and those described by (33, 34) are *not* mutually exclusive. Indeed, it is very likely that the proximal to distal organization of functional subunits described by (33, 34) is a feature of each of the dendritic trajectories examined in the present study. Thus, the dendritic trees of neck motoneurons may be divided into functional subunits according to the trajectory followed by the dendrite *and* the distance to the soma.

The dependency between the functional properties of motoneuron dendrites and their trajectory has another counterpart. Descending axons from neurons in the lateral vestibular nucleus preferentially contact rostrally and caudally directed dendrites of BCCM and splenius motoneurons (44). In contrast, synapses from the neighboring descending vestibular nucleus are largely found on dendrites projecting laterally, dorsolaterally, medially, and dorsomedially. Thus, these connections adopt the same trajectory dependency as found in the present study. Assuming that synapses from these nuclei generate equivalent changes in conductance, the trajectory dependency of the signal transmission properties of the dendrites of BCCM motoneurons leads to the prediction that connections from the descending vestibular nucleus are strategically located to deliver more current to the soma compared to connections from the lateral vestibular nucleus.

Trajectory dependence is not a unique feature of connections to neck motoneurons. Contacts between Ia afferents and dendrites of hindlimb motoneurons are also arranged in a trajectory-dependent fashion, albeit not as striking as the pattern between vestibulospinal terminals and dendrites of neck motoneurons (9). It has been suggested that the degree of non-linear interactions between Ia afferents and other synaptic inputs to hindlimb motoneurons may also be related to dendritic trajectory (49). Thus, the trajectories followed by motoneuron dendrites serve as a common organizational framework for synaptic distribution patterns, synaptic integration, *and* efficacy of signal transmission. This is not to say that dendritic trajectory is the sole factor governing all of these parameters. Thus, the accumulating evidence for trajectory-based features provides a strong justification for concluding that the wide functional diversity of motoneuron dendrites is not an accident. Instead, this feature of motoneuron dendrites may be part of a larger strategy that ensures that the output of the motoneuron is matched to the properties of its inputs.

SUMMARY

The distribution and geometry of the dendritic trees of spinal motoneurons obey several well-established rules. Some of these rules are based on systematic relationships between quantitative geometrical features (e.g. total dendritic length) and the three-dimensional trajectory followed by dendrites from their origin to their termination. Since dendritic geometry partially determines the transmission of current and voltage signals generated by synapses on the dendritic tree, our goal was to compare the efficacy of signal transmission by dendritic trajectories that followed different directions. To achieve this goal, we constructed detailed compartmental models of the dendritic trees of intracellularly stained neck motoneurons and calculated the electrotonic properties of each soma-to-terminal trajectory. These properties displayed a high degree of variability. To determine if this variability was due, in part, to the orientation (e.g. rostral, rostral-dorsal-lateral) of the trajectory, each trajectory was classified according to its orientation. The attenuation of current and voltage signals en route to the soma were strongly related to trajectory orientation. Trajectories with similar attenuation factors formed functional subunits that were arranged in distinct domains within the ventral horn. The difference in the efficacy of signal transmission between subunits was increased by activation of neighbouring synapses due to trajectory-related differences in non-linear summation. These results indicate that the input-output properties of motoneurons depend on the direction of the path taken by dendrites from their origin at the cell body to their terminals.

Acknowledgments. This research was supported by the Canadian Institutes for Health Research (MOP-37765) and the National Institutes of Health ((RO1 NS40850).

REFERENCES

1. BERNANDER, O., DOUGLAS, R.J., MARTIN, K.A., AND KOCH, C. Synaptic background activity influences spatiotemporal integration in single pyramidal cells. *Proc. Natl. Acad. Sci. USA*, **88**: 11569-11573, 1991.
2. BINDER, M.D., HECKMAN, C.J. AND POWERS, R.K. The physiological control of motoneuron activity. In: ROWELL, L.B. AND SHEPHERD, T.J. (Eds.), *Handbook of Physiology. Section 12. Exercise: Regulation and Integration of Multiple Systems*. New York, Oxford University Press, 1996, pp. 3-53.
3. BIRINYI, A., ANTAL, M., WOLF, E., AND SZEKELY, G. The extent of the dendritic tree and the number of synapses in the frog motoneuron. *Eur. J. Neurosci.*, **4**: 1003-1012, 1992.
4. BRAS, H., GOGAN, P., AND TYC-DUMONT, S. The dendrites of single brain-stem motoneurons intracellularly labelled with horseradish peroxidase in the cat. Morphological and electrical differences. *Neurosci.*, **22**: 947-970, 1987.
5. BRAS, H., KOROGOD, S., DRIENCOURT, Y., GOGAN, P., AND TYC-DUMONT, S. Stochastic geometry and electronic architecture of dendritic arborization of brain stem motoneuron. *Eur. J. Neurosci.*, **5**: 1485-1493, 1993.
6. BROWN, A.G. AND FYFFE, R.E.W. Direct observations on the contacts made between Ia afferent fibers and a-motoneurons in the cat's lumbosacral spinal cord. *J. Physiol., Lond.*, **313**: 121-140, 1981.
7. BUI, T., CUSHING, S., DEWEY, D., FYFFE, R.E., AND ROSE, P.K. A comparison of the elec-

trotonic and morphological properties of Renshaw cells, Ia inhibitory interneurons, and motoneurons in the cat. *J. Neurophysiol.*, **90**: 2900-2918, 2003.

8. BUI, T.V., TER-MIKHAELIAN, M., BEDROSSIAN, D., AND ROSE, P.K. Computational estimation of the distribution of L-type Ca²⁺ channels in motoneurons based on variable threshold of activation of persistent inward currents. *J. Neurophysiol.*, **95**: 225-241, 2006.
9. BURKE, R.E. AND GLENN, L.L. Horseradish peroxidase study of the spatial and electrotonic distribution of group Ia synapses on type-identified ankle extensor motoneurons in the cat. *J. Comp. Neurol.*, **372**: 465-485, 1996.
10. BURKE, R.E., MARKS, W.B., AND ULFHAKE, B. A parsimonious description of motoneuron dendritic morphology using computer simulation. *J. Neurosci.*, **12**: 2403-2416, 1992.
11. CAMERON, W.E., AVERILL, D.B., AND BERGER, A.J. Morphology of cat phrenic motoneurons as revealed by intracellular injection of horseradish peroxidase. *J. Comp. Neurol.*, **219**: 70-80, 1983.
12. CAMERON, W.E., AVERILL, D.B., AND BERGER, A.J. Quantitative analysis of the dendrites of cat phrenic motoneurons stained intracellularly with horseradish peroxidase. *J. Comp. Neurol.*, **230**: 91-101, 1985.
13. CAPOWSKI, J.J. Computer techniques in neuroanatomy, New York, Kluwer, 1989.
14. CARNEVALE, N.T., WOOLF, T.B., AND SHEPHERD, G.M. Neuron simulations with SABER. *J. Neurosci. Methods.*, **33**: 135-148, 1990.
15. CHEN, X.Y. AND WOLPAW, J.R. Triceps surae motoneuron morphology in the rat: A quantitative light microscopic study. *J. Comp. Neurol.*, **343**: 143-157, 1994.
16. CLEMENTS, J.D. AND REDMAN, S.J. Cable properties of cat spinal motoneurons measured by combining voltage clamp, current clamp and intracellular staining. *J. Physiol., Lond.*, **409**: 63-87, 1989.
17. CULLHEIM, S., FLESHMAN, J.W., GLENN, L.L., AND BURKE, R.E. Membrane area and dendritic structure in type-identified triceps surae alpha motoneurons. *J. Comp. Neurol.*, **255**: 68-81, 1987.
18. CULLHEIM, S., FLESHMAN, J.W., GLENN, L.L., AND BURKE, R.E. Three-dimensional architecture of dendritic trees in type-identified alpha-motoneurons. *J. Comp. Neurol.*, **255**: 82-96, 1987.
19. CUSHING, S., BUI, T., AND ROSE, P.K. Effect of nonlinear summation of synaptic currents on the input-output properties of spinal motoneurons. *J. Neurophysiol.*, **94**: 3465-3478, 2005.
20. DITYATEV, A.E., CHMYKHOVA, N.M., STUDER, L., KARAMIAN, O.A., KOZHANOV, V.M., AND CLAMANN, H.P. Comparison of the topology and growth rules of motoneuronal dendrites. *J. Comp. Neurol.*, **363**: 505-516, 1995.
21. FINKEL, A.S. AND REDMAN, S.J. The synaptic current evoked in cat spinal motoneurons by impulses in single group Ia axons. *J. Physiol., Lond.*, **342**: 615-632, 1983.
22. GRANIT R., KERNELL D. AND SHORTESS G.K. Quantitative aspects of repetitive firing of mammalian motoneurons, caused by injecting currents. *J. Physiol., Lond.*, **168**: 911-931, 1963.
23. GRANIT, R., KERNELL, D. AND LAMARRE, Y. Algebraical summation in synaptic activation of motoneurons firing within the 'primary range' to injected currents. *J. Physiol., Lond.*, **187**: 379-399, 1966.
24. FYFFE, R.E.W. Spatial distribution of recurrent inhibitory synapses on spinal motoneurons in the cat. *J. Neurophysiol.*, **65**: 1134-1149, 1991
25. HECKMAN, C.J. AND BINDER, M.D. Analysis of effective synaptic currents generated by homonymous Ia afferent fibers in motoneurons of the cat. *J. Neurophysiol.*, **60**: 1946-1966, 1988.
26. HECKMAN, C.J., LEE, R.H. AND BROWNSTONE, R.M. Hyperexcitable dendrites in motoneurons and their neuromodulatory control during motor behavior. *Trends Neurosci.*, **26**: 688-695, 2003.

27. JAEGER, D. Accurate reconstruction of neuronal morphology. In DE SCHUTTER, E., (Ed.). Computational Neuroscience Realistic Modeling for Experimentalists. London, CRC Press, 2001, pp. 159-178.
28. JAFFE, D.B. AND CARNEVALE, N.T. Passive normalization of synaptic integration influenced by dendritic architecture. *J. Neurophysiol.*, **82**: 3268-3285, 1999.
29. KEIRSTEAD, S.A. AND ROSE, P.K. Dendritic distribution of splenius motoneurons in the cat: comparison of motoneurons innervating different regions of the muscle. *J. Comp. Neurol.*, **219**: 273-284, 1983.
30. KERNELL, D. AND ZWAAGSTRA, B. Dendrites of cat's spinal motoneurons: relationship between stem diameter and predicted input conductance. *J. Physiol., Lond.*, **413**: 255-269, 1989.
31. KERNELL, D. AND ZWAAGSTRA, B. Size and remoteness: two relatively independent parameters of dendrites, as studied for spinal motoneurons of the cat. *J. Physiol., Lond.*, **413**: 233-254, 1989.
32. KOCH, C. Biophysics of Computation. New York, Oxford University Press, 1999.
33. KOROGOD, S., BRAS, H., SARANA, V.N., GOGAN, P., AND TYC-DUMONT, S. Electrotonic clusters in the dendritic arborization of abducens motoneurons of the rat. *Eur. J. Neurosci.*, **6**: 1517-1527, 1994.
34. KOROGOD, S.M., KULAGINA, I.B., HORCHOLLE-BOSSAVIT, G., GOGAN, P., AND TYC-DUMONT, S. Activity-dependent reconfiguration of the effective dendritic field of motoneurons. *J. Comp. Neurol.*, **422**: 18-34, 2000.
35. McDONAGH, J.C., HORNBLY, T.G., REINKING, R.M., AND STUART, D.G. Associations between the morphology and physiology of ventral-horn neurons in the adult turtle. *J. Comp. Neurol.*, **454**: 177-191, 2002.
36. OKADO, N., HOMMA, S., ISHIHARA, R., AND KOHNO, K. Distribution patterns of dendrites in motor neuron pools of lumbosacral spinal cord of the chicken. *Anat. Embryol., Berl.*, **182**: 113-121, 1990.
37. POWERS, R.K. AND BINDER, M.D. Input-output functions of mammalian motoneurons. *Rev. Physiol. Biochem. Pharmacol.*, **143**: 137-263, 2001.
38. RALL, W. Core conductor theory and cable properties of neurons. In BROOKHART, J.M. AND MOUNTCASTLE, V.B., editors. Handbook of Physiology. Section I: The Nervous System. Bethesda, American Physiological Society, 1977, pp 39-98.
39. RALL, W. AND RINZEL, J. Branch input resistance and steady attenuation for input to one branch of a dendritic neuron model. *Biophys. J.*, **13**: 648-687, 1973.
40. RAMÓN Y CAJAL. Histologie du Système Nerveux de L'homme et des Vertébrés. Paris, A. Maloine, 1909.
41. ROSE, P.K. Distribution of dendrites from biventer cervicis and complexus motoneurons stained intracellularly with horseradish peroxidase in the adult cat. *J. Comp. Neurol.*, **197**: 395-410, 1981.
42. ROSE P.K. Branching structure of motoneuron stem dendrites: a study of neck muscle motoneurons intracellularly stained with horseradish peroxidase in the cat. *J. Neurosci.*, **2**: 1596-1607, 1982.
43. ROSE, P.K. AND CUSHING, S. The relationship between morphoelectrotonic properties of motoneuron dendrites and their trajectory. *J. Comp. Neurol.*, **473**: 562-581, 2005.
44. ROSE, P.K., JONES, T., NIRULA, R., AND CORNEIL, T. Innervation of motoneurons based on dendritic orientation. *J. Neurophysiol.*, **73**: 1319-1322, 1995.
45. ROSE P.K., KEIRSTEAD S.A., AND VANNER S. A quantitative analysis of the geometry of cat motoneurons innervating neck and shoulder muscles. *J. Comp. Neurol.*, **239**: 89-107, 1985.
46. ROSE P.K. AND NEUBER-HESS M. Morphology and frequency of axon terminals on the

- somata, proximal dendrites, and distal dendrites of dorsal neck motoneurons in the cat. *J. Comp. Neurol.*, **307**: 259-280, 1991.
47. ROSE, P.K. AND ODLOZINSKI, M. Expansion of the dendritic tree of motoneurons innervating neck muscles of the adult cat after permanent axotomy. *J. Comp. Neurol.*, **390**: 392-411, 1998.
 48. SCHWINDT, P.C. AND CALVIN, W.H. Equivalence of synaptic and injected current in determining the membrane potential trajectory during motoneuron rhythmic firing. *Brain Res.*, **59**: 389-394, 1973.
 49. SEGEV, I., FLESHMAN, J.W., JR., AND BURKE, R.E. Computer simulation of group Ia EPSPs using morphologically realistic models of cat alpha-motoneurons. *J. Neurophysiol.*, **64**: 648-660, 1990.
 50. STUART, G.J. AND REDMAN, S.J. Voltage dependence of Ia reciprocal inhibitory currents in cat spinal motoneurons. *J. Physiol., Lond.*, **420**: 111-125, 1990.
 51. ULFHAKKE, B. AND KELLERTH, J.-O. A quantitative light microscopic study of the dendrites of cat a-motoneurons after intracellular staining with horseradish peroxidase. *J. Comp. Neurol.*, **202**: 571-583, 1981.
 52. ULFHAKKE, B. AND KELLERTH, J.-O. A quantitative morphological study of HRP-labelled cat a-motoneurons supplying different hindlimb muscles. *Brain Res.*, **264**: 1-20, 1983.
 53. VANNER, S.J. AND ROSE, P.K. Dendritic distribution of motoneurons innervating the three heads of the trapezius muscle in the cat. *J. Comp. Neurol.*, **226**: 96-110, 1984.
 54. WALMSLEY, B., ALVAREZ, F.J. AND FYFFE, R.E. Diversity of structure and function at mammalian central synapses. *Trends Neurosci.*, **21**: 81-88, 1998.
 55. WESTERGA, J. AND GRAMSBERGEN, A. Structural changes of the soleus and the tibialis anterior motoneuron pool during development in the rat. *J. Comp. Neurol.*, **319**: 406-416, 1992.

